agriculture

Article

Using UAV Multispectral Imagery to Predict Leaf SPAD Dynamics During Maize Growth Under Different Plant Densities

Cheng Li [1], Li Dai [1], Zihan Zeng [1], Junjie Huang [1], Huihui Liu [1], Shan Jiang [2,3], Jincai Li [1,*] and Youhong Song [1,4,5]

1 School of Agronomy, Anhui Agricultural University, Hefei 230036, China; y.song@ahau.edu.cn (Y.S.)
2 Universities Joint Key Laboratory of Photoelectric Detection Science and Technology in Anhui Province, Hefei Normal University, Hefei 230601, China
3 College of Physics and Material Engineering, Hefei Normal University, Hefei 230601, China
4 Key Laboratory of Crop Physiology, Ecology and Genetic Breeding, Ministry of Education, Jiangxi Agricultural University, Nanchang 330045, China
5 Centre for Crop Science, Queensland Alliance for Agriculture and Food Innovation, The University of Queensland, Brisbane, QLD 4350, Australia
* Correspondence: ljc5122423@126.com

Abstract

Chlorophyll content represents a key growth indicator for maize. The traditional SPAD (Soil and Plant Analyzer Development) method, though easy to operate, is inefficient, destructive, and unsuitable for high-throughput field monitoring. UAV (Unmanned Aerial Vehicle) remote sensing technology is highly efficient and detects abundant indicators, enabling large-scale SPAD measurement. In this study, 18 vegetation indices and eight texture features were selected as the indicator system by combining prior knowledge and experimental analysis. In a two-year maize density experiment, multispectral images were collected in the growth period. The correlations among SPAD values, multispectral indices and texture features were analyzed using Pearson correlation coefficients. Then the detection accuracies of three algorithms, i.e., RF (Random Forest), PLSR (Partial Least Squares Regression), and SVR (Support Vector Regression), were compared under this indicator system. Compared with models constructed using single vegetation indices or single texture features, the estimation accuracy of the indicator system at the jointing stage was improved by 0.13 and 0.22, respectively. The results showed that SVR achieved the highest estimation accuracy among the three algorithms, with determination coefficients (R^2) of 0.73, 0.77and 0.70 at the jointing, silking, and grain-filling stages, respectively. This study established a non-destructive monitoring framework for chlorophyll content during the entire maize growth stage based on UAV data.

Keywords: *Zea mays* L.; plant density; SPAD estimation; UAV; machine learning

Academic Editor: Mavromatis Theodoros

Received: 26 May 2026
Revised: 25 June 2026
Accepted: 29 June 2026
Published: 1 July 2026

1. Introduction

Maize (*Zea mays* L.) is an important crop because of its suitability for a variety of purposes, such as food, energy consumption and animal feeds [1]. Leaf nitrogen content is a core indicator for maize nutrition and vigor diagnosis [2]. SPAD values can quantitatively characterize crop nitrogen nutrition and chlorophyll levels, which is critical for precise nitrogen application and yield management [3,4]. Traditional manual measurement is labor intensive and cannot meet modern agricultural monitoring needs [5], while UAV multispectral remote sensing enables efficient non-destructive SPAD inversion, serving as a key tool for precision agriculture monitoring [6,7].

In recent years, UAV-borne multispectral remote sensing has been increasingly applied in precision agriculture, especially for the inversion of crop SPAD values. It is difficult to construct a stable inversion model for the entire growth period relying solely on single spectral information [8]. The key lies in constructing stable and highly generalizable estimation models suitable for multi-variety, multi-region, and multi-climate scenarios. Various Vis (Vegetation Indices) derived from canopy reflectance have been successfully applied to chlorophyll estimation and crop growth evaluation [9,10]. However, crop spectral characteristics change continuously throughout the entire growth period, and their correlation with chlorophyll content also varies accordingly. It is difficult to construct a stable inversion model for the growth period relying solely on single spectral information. Image texture features can effectively compensate for the deficiencies of spectral information, providing a new approach to solving this problem.

Texture features extracted from remote sensing images can quantitatively describe the spatial distribution and structural heterogeneity of crop canopies [11]. Therefore, in spectral inversion, they effectively alleviate the signal saturation problem of traditional VIs under high canopy closure and compensate for the instability of spectral signals caused by variations in growth stages and environmental conditions. By integrated VIs with texture features, the accuracy, stability, and generalization ability of physiological parameter inversion models can be significantly improved [12]. In agricultural applications, texture features have been widely used in non-destructive monitoring of crop growth, SPAD estimation [13], yield prediction [14] and stress detection. They provide critical spatial structural information that spectra alone cannot capture, especially for dense planting populations. Therefore, integrating texture features into remote sensing inversion has become an important means to promote high-precision and intelligent monitoring in precision agriculture.

However, most existing studies focus on a single growth stage or specific environmental conditions. The limited research on SPAD estimation models for the summer maize during entire growth cycle under various field conditions is still a core challenge. This study aimed to explore the feasibility of accurately estimating maize canopy SPAD values in the growth period using multispectral remote sensing. A total of 12,240 UAV multispectral images were collected over two years under different maize planting densities. Based on the correlations among SPAD values, VIs, and texture features, 18 VIs and eight texture features were extracted to construct an indicator system for SPAD values estimation from UAV remote sensing imagery. The estimation accuracies of three algorithms were compared, confirming SVR as the optimal one, and its feasibility for estimating maize canopy SPAD values under field conditions was verified.

2. Materials and Methods

2.1. Experiment Location and Design

Field trials were conducted at the Mengcheng County Agricultural Technology Demonstration Farm in Bozhou City, Anhui Province, China (33°9′ N, 116°32′ E). In this study, we used two widely grown maize cultivars in the Huang-Huai-Hai region, i.e., ZD958 and MY73, and set up four planting densities, i.e., PD3 (30,000 plants ha^{-1}), PD6 (60,000 plants ha^{-1}), PD9 (90,000 plants ha^{-1}), and PD12 (120,000 plants ha^{-1}). Image data were collected during the 2023 and 2024 maize growing seasons using a DJI M300 RTK UAV (DJI Innovations Science and Technology Co. Ltd., Shenzhen, China) equipped with an AQ600 Pro multispectral sensor (Changguang Yuchen Information Technology and Equipment Co. Ltd., Qingdao, China). The AQ600 Pro is a standard professional UAV

https://doi.org/10.3390/agriculture16131442

multispectral camera equipped with 5 multispectral channels (3.2 megapixels per channel) and 1 RGB channel (12.3 megapixels). Multispectral data preprocessing was performed using DJI Terra (v5.0.2). Band math, region of interest (ROI) definition and pixel statistics were conducted in ENVI 5.3 software to extract the average reflectance of each plot, which was used as the spectral reflectance sample for each band. A total of 12,240 multispectral images of maize during the growth period (covering V3, V6, V10, V12, VT, R1, R2, and R3) were collected in field conditions. Subsequently, this study constructed a representative dataset named SPADmaize_ahau, with the 2025 dataset used as the training set and the 2024 dataset as the test set to verify the generalization ability of the model under interannual climatic conditions.

To verify the accuracy of SPAD values retrieved by remote sensing, the SPAD-502 chlorophyll meter (Konica Minolta, Ltd., Tokyo, Japan) was used to measure ground-based SPAD values synchronously with remote sensing data acquisition, so as to characterize the chlorophyll content of summer maize. The measurement accuracy of the instrument was ±1.0 SPAD units, and the repeatability error was ±0.3 SPAD units. Uniform-growth maize plants were randomly selected in each experimental plot, with 10 plants sampled per treatment. Fully expanded leaves with uniform light exposure, no pests, diseases or mechanical damage were selected as target leaves during measurement, and SPAD readings were separately measured at the leaf tip, middle and basal positions. The average of these three measurements was defined as the final SPAD value for each leaf of the corresponding treatment. All SPAD measurements were conducted between 9:00 and 11:00 a.m. under clear and cloudless weather conditions to eliminate the influence of varying light conditions on measured values. Field SPAD measurements and UAV remote sensing data acquisition were completed on the same day to guarantee the temporal and spatial matching between ground truth measurements and remote sensing spectral information (Figure 1).

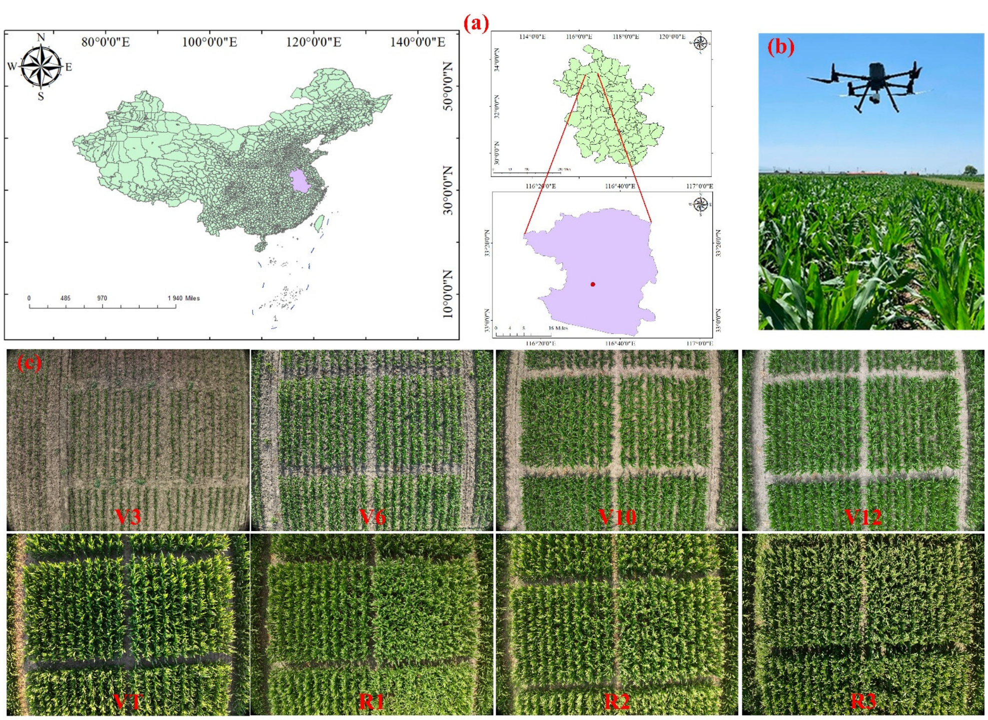

Figure 1. Illustration of the experimental procedure. (**a**) Field trial in Bozhou, Anhui. (**b**) UAV multispectral data collection. (**c**) Multispectral images of maize growth stages.

2.2. Indicator System

VIs play a dominant role in SPAD inversion by reflecting crop biochemical information, while texture features provide supplementary spatial structural details of the canopy. The integration of these two types of features can effectively improve estimation accuracy.

Drawing on prior findings and the responsiveness of chlorophyll content to spectral features, this work selected the indices listed in Table 1 to explore their correlation with SPAD values in summer maize. Meanwhile, all feasible texture indicators integrated were constructed across five spectral bands (450, 560, 650, 730, and 840 nm). A total of eight texture features based on the Gray-Level Co-occurrence Matrix (GLCM) were used: mean (mean), variance (var), homogeneity (hom), contrast (con), dissimilarity (dis), entropy (ent), second moment (sm), and correlation (cor). Multi-featured integration effectively compensates for the limitations of single spectral or texture information, which is crucial for improving the accuracy and stability of SPAD simulation. Detailed information on the texture features corresponding to each spectral band is provided in Table 2.

To avoid model overfitting and distorted parameter estimation caused by ignoring collinearity among variables, we performed a Variance Inflation Factor (VIF) test on the feature sets screened for each core model. The VIF values of vegetation indices and texture features ranged from 1.35 to 4.34, which were far below the empirical threshold of 10, indicating no severe multicollinearity among the selected features. L1 regularization was applied to conduct sparse feature selection. The results revealed that the intersection ratio between features retained by LASSO and those screened via Pearson correlation analysis ($|r| > 0.6$) ranged from 82% to 91% (with slight variations across different growth stages). The coefficient of determination R^2 of the SVR model built on LASSO-selected features (0.70–0.75) was close to that of the model using Pearson-screened features (0.72–0.77), and no statistically significant difference was observed between the two approaches ($p > 0.05$). Recursive Feature Elimination (RFE) combined with cross-validation was used to iteratively eliminate non-essential features. The results demonstrated that the optimal feature subset obtained by RFE shared an overlap of more than 78% with the Pearson-screened feature set. Furthermore, the features with the highest Pearson correlation coefficients (such as MCCCI and entropy) were also prioritized and retained in the RFE feature ranking.

Table 1. The 18 VIs used in this study.

Acronym	Vegetation Index	Formula	Reference
NDVI	Normalized Difference Vegetation Index	NDVI = (NIR − Red)/(NIR + Red)	[15]
NDRE	Normalized Difference Red-Edge Vegetation Index	NDRE = (NIR − Red Edge)/(NIR + Red Edge)	[16]
MSRI	Modified Simple Ratio Index	MSRI = (NIR/R − 1)/sqrt(NIR/R + 1)	[17]
GNDVI	Green Normalized Difference Vegetation Index	GNDVI = (NIR − Green)/(NIR + Green)	[18]
OSAVI	Optimized Soil Adjusted Vegetation Index	OSAVI = (NIR−Red)/(NIR + Red + 0.16) × 1.16	[19]
EVI	Enhanced Vegetation Index	EVI = 2.5 × (NIR − Red)/(NIR + 2.4 × Red + 1)	[20]
TNDVI	Transformed Normalized Difference Vegetation Index	TNDVI = sqrt(NIR − Red Edge)/(NIR + Red Edge) + 0.5	[21]
GOSAVI	Green Optimized Soil Adjusted Vegetation Index	GOSAVI = 1.16 × (NIR − Green)/(NIR + Green + 0.16)	[22]
GDVI	Green Difference Vegetation Index	GDVI = NIR − Green	[23]
RVI	Ratio Vegetation Index	RVI = NIR/Red	[24]
DVI	Deviation Vegetation Index	DVI = NIR − Red	[25]
SR	Simple Ratio (SR)	SR = NIR/Red	[26]
NGI	Normalized Green Vegetation Index	NGI = Red/(NIR + Red Edge + Red)	[27]

MCCCI	Modified Climate Change Canopy Vegetation Index	MCCCI = (NIR − Red Edge)/(NIR + Red Edge)	[28]
MTCI	MERIS Terrestrial Chlorophyll Index	MTCI = (NIR − Red Edge)/(Red Edge − Red)	[29]
CIgreen	Green Chlorophyll Index	CIgreen= NIR/Red − 1	[30]
VIopt	Optimal Vegetation Index	VIopt = 1.45 × ((Red^2 + 1)/(Red + 0.45))	[31]
DATT	Datt1	DATT = (NIR − Red Edge)/(NIR − Red)	[32]

Table 2. Examining relationships of single texture features with each spectral band in the rise period.

Texture Feature	Correlation Coefficient				
	Blue	**Green**	**Red**	**Red Edge**	**Near IR**
Mean (mean)	−0.10	−0.08	−0.15	0.07	0.18
Correlation (corr)	0	−0.08	0.07	−0.19	−0.17
Dissimlarity (dis)	−0.10	−0.06	−0.15	0.09	0.20
Angular (ang)	0.7	0.58	0.82	0.04	−0.71
Variance (var)	−0.05	−0.04	−0.10	0.06	0.12
Contrast (con)	−0.06	−0.03	−0.08	0.07	0.12
Entropy (ent)	−0.68	−0.55	−0.80	0.04	0.75
Homogeneity (hom)	0.56	0.34	0.62	−0.16	−0.62

2.3. Model Selection

Multi-featured integration effectively compensates for the limitations of single spectral or texture information, which is crucial for improving the accuracy and stability of SPAD estimation. Previous studies have widely applied the SVR algorithm to handle multi-feature integrated tasks in the retrieval of vegetation physiological parameters. As a core algorithm branch of SVM (Support Vector Machine) for regression tasks, SVR is a classic machine learning method based on the structural risk minimization principle, which achieves data fitting and continuous value prediction by constructing an ε-insensitive loss function. In the remote sensing inversion modeling of maize canopy SPAD based on multi-feature integration, the SVR model presents strong adaptability to high-dimensional fused features, fully integrating the complementary information of spectral and texture features. It significantly outperforms conventional regression algorithms in terms of SPAD estimation accuracy, model stability and cross-scene generalization ability. For multi-feature integrated modeling, SVR effectively mitigates the curse of dimensionality and overfitting in the small-sample high-dimensional feature space, and its superior nonlinear fitting ability fully exploits the intrinsic relationship between multi-source features and SPAD values to maximize the performance of multi-feature integration. The model performance was then evaluated using SPADmaize_ahau (Figure 2).

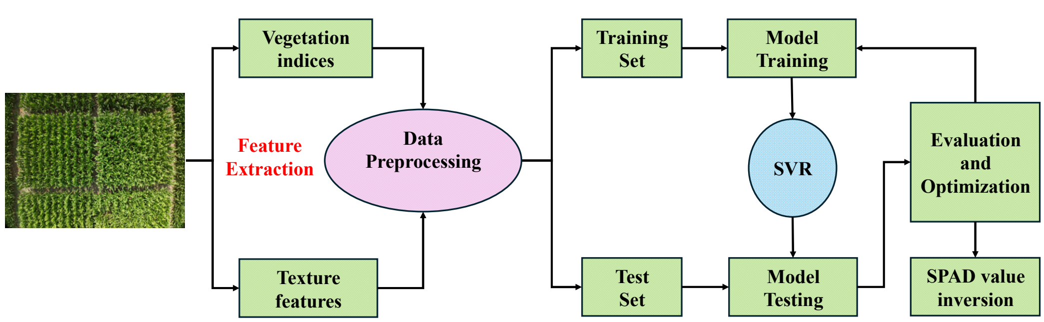

Figure 2. Flowchart of SPAD inversion using VIs and texture features.

In this study, the performance of the SPAD inversion models was evaluated using two accuracy metrics: Root Mean Squared Error (*RMSE*) and Coefficient of Determination (R^2). A value of R^2 closer to 1 indicates a better model fit. Meanwhile, a lower *RMSE* corresponds to smaller prediction errors, representing higher overall accuracy and more robust estimation performance. The calculation formulas are as follows.

$$R^2 = 1 - \frac{\sum_{i=1}^{n}(y_i - \hat{y}_i)^2}{\sum_{i=1}^{n}(y_i - \bar{y}_i)^2} \quad (1)$$

$$RMSE = \sqrt{\frac{1}{n}\sum_{i=1}^{n}(y_i - \hat{y}_i)^2} \quad (2)$$

$$MSE = \frac{1}{n}\sum_{i=1}^{n}(y_i - \hat{y}_i)^2 \quad (3)$$

where y_i denotes the measured SPAD value, $\hat{y}_i$ is the model's prediction, $\bar{y}$ signifies the mean observed value, and n represents the total number of samples. Together, these indices serve to gauge the model's performance, delivering insights into its accuracy and estimation power across multiple dimensions.

2.4. Validation Strategy

Within the interannual validation framework, leave-one-growth-stage-out validation was additionally performed across key maize growth stages including the tasseling stage, filling stage, and maturity stage to evaluate the model's adaptability across different developmental phases and prevent model training from being dominated by data from a single specific growth stage. Given that planting density served as a core regulatory factor in this study, we implemented independent grouped validation for each density treatment. Specifically, datasets from partial density treatments were adopted for model training, and the trained model was then tested on datasets from density treatments that were not involved in the training process, aiming to examine the model's transferability to unseen planting density levels.

2.5. Hyperparameter Tuning

In this study, grid search combined with K-fold cross-validation was adopted for hyperparameter tuning. Grid search exhaustively traverses all combinations within the predefined parameter space and evaluates the performance of each parameter set via cross-validation to determine the globally optimal parameter combination. The key hyperparameters of different algorithms are shown in Figure 3 and Table 3.

Table 3. Key hyperparameters of the three algorithms.

Algorithm	Hyperparameter	Search Range	Search Step Size
SVR	Penalty coefficient C	[0.1, 1, 10, 100, 1000]	log-spaced
	Kernel function parameter γ	[0.001, 0.01, 0.1, 1, 10]	log-spaced
	Insensitive loss function parameter ε	[0.001, 0.01, 0.05, 0.1, 0.5]	linearly spaced
RF	n_estimators	[50, 100, 200, 300, 500]	
	max_depth	[5, 10, 15, 20, 30, None]	
	min_samples_split	[2, 5, 10]	
	min_samples_leaf	[1, 2, 4]	
PLSR	n_components	[1, 2, 3, …, 20]	

https://doi.org/10.3390/agriculture16131442

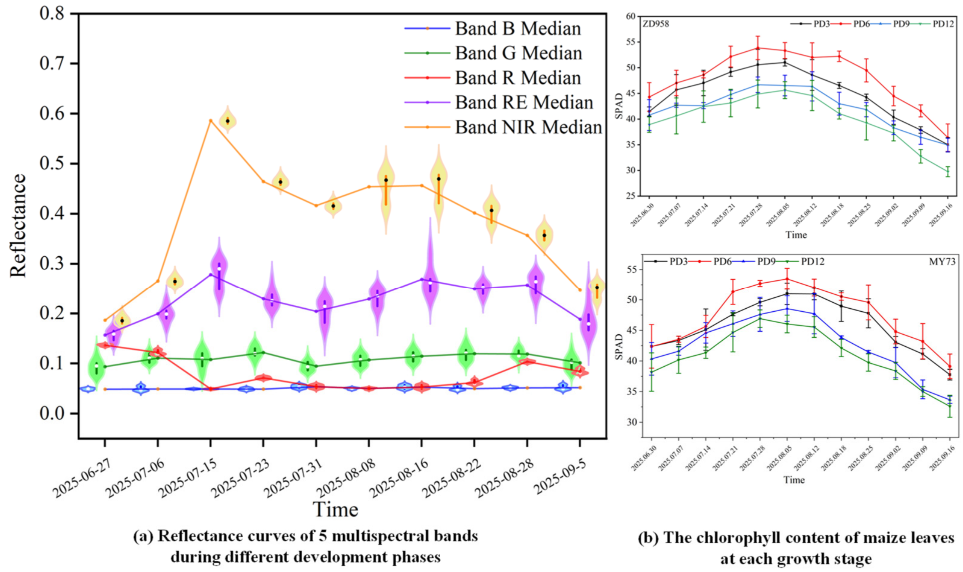

Figure 3. Dynamics of SPAD values and multi-band spectral reflectance characteristics of summer maize during maize growth period. Note: PD3 (30,000 plants ha^{-1}), PD6 (60,000 plants ha^{-1}), PD9 (90,000 plants ha^{-1}), PD12 (120,000 plants ha^{-1}). Error bars indicate standard deviation.

Hyperparameter tuning was performed using 5-fold cross-validation in this study. The GridSearchCV module embedded in the Scikit-learn library of Python 3.9 was employed to realize the joint optimization of grid search and cross-validation. To balance computational efficiency and search accuracy, a two-stage strategy consisting of coarse-grained search followed by fine-grained search was adopted. First, a large search range with a relatively large step size was used to locate the approximate interval of optimal hyperparameters. Subsequently, a fine search with a small step size was implemented around this optimal interval to obtain the final optimal parameter combination.

3. Results

3.1. Chlorophyll Content at Different Growth Stages

To accurately characterize the dynamic trend of leaf chlorophyll content during the maize entire growth period and facilitate comparative experiments with remote sensing data, the SPAD values measured using SPAD-502 are presented in Figure 3b, while the temporal variations in reflectance across five multispectral bands are recorded in Figure 3a. The SPAD value of maize exhibits a unimodal trend throughout the entire growth period, increasing initially and peaking at the flowering and grain-filling stage, followed by a rapid decline in the late growth stage. This dynamic pattern is highly coupled with the temporal variation of reflectance across the five multispectral bands. Specifically, the reflectance of the near-infrared (NIR), red-edge (RE), and green (G) bands shows a significant positive correlation with SPAD values; displaying a fully synchronous temporal trend, their reflectance remains at a high level, with the smallest fluctuation during the SPAD peak period. In contrast, the reflectance of the red (R) and blue (B) bands is negatively correlated with SPAD values, decreasing as SPAD increases and exhibiting an opposite trend in the late growth stage. Since most VIs are constructed from the integration of these chlorophyll-sensitive bands, they can effectively amplify the correlation between spectral signals and SPAD values. Consequently, VIs demonstrates a strong correlation with SPAD values and serves as core input indicators for SPAD remote sensing inversion in summer maize.

3.2. Correlation Analysis Among VIs, Texture Features and SPAD Values

For scenarios where the canopy closes and VIs generally suffer spectral saturation during the mid-to-late growth stages of maize, texture features can overcome the limitation of spectral saturation by capturing differences in spatial heterogeneity, thereby enabling effective inversion of chlorophyll content. However, across the entire growth period, the correlation between VIs and SPAD values is significantly stronger than that of texture features. Therefore, to evaluate their correlations, this study conducted correlation analyses among measured SPAD values, VIs and texture features. The results at the jointing stage are presented in Figure 4 and Table 4, with detailed information provided in Supplementary. The results showed that most VIs were extremely significantly correlated with SPAD values at each growth stage ($p < 0.001$). Red-edge vegetation indices presented the optimal performance at the jointing stage, with correlation coefficients of DATT and MTCI reaching 0.67, and those of NDRE, CIre and other red-edge indices all exceeding 0.62, while the green band showed an extremely strong negative correlation with SPAD (r = −0.70). Red-edge indices remained sensitive to chlorophyll changes at the silking stage, with correlation coefficients of DATT, NDRE and CIre of 0.55, 0.52 and 0.52, respectively. The correlation between near-infrared integrated vegetation indices and SPAD increased significantly at the grain-filling stage, with correlation coefficients of RVI, VIopt, OSAVI and other indices all exceeding 0.75, and the red band showed a strong negative correlation with SPAD (r = −-0.71). This study clarified the optimal VIs for SPAD inversion of summer maize at different growth stages and provided reliable technical support for non-destructive field monitoring of nitrogen nutrition throughout the growth period.

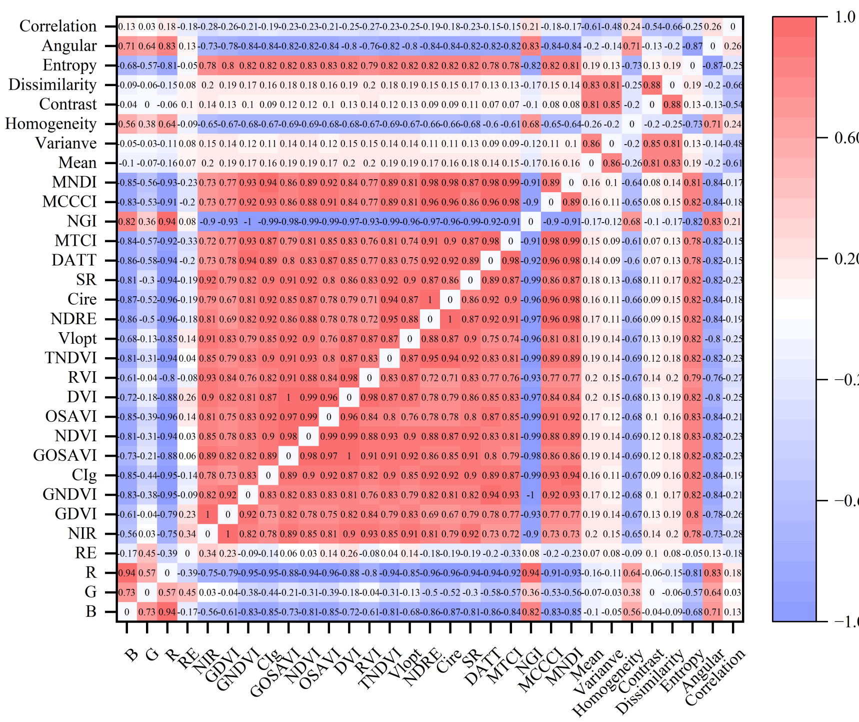

Figure 4. The interplay of spectral and SPAD features: a correlation assessment during the jointing stage.

Table 4. Correlation analysis between each spectral index and SPAD during maize jointing stage.

Spectral Index	Correlation Coefficient	Spectral Index	Correlation Coefficient
B	−0.55 ***	DVI	0.44 ***
G	−0.70 ***	TNDVI	0.38 ***
R	−0.60 ***	VIopt	0.49 ***
RE	−0.45 ***	RVI	0.45 ***
NIR	0.33 ***	NDRE	0.62 ***
GDVI	0.40 ***	Cire	0.62 ***
GNDVI	0.58 ***	SR	0.49 ***
CIg	0.60 ***	DATT	0.67 ***
GOSAVI	0.50 ***	MTCI	0.67 ***
NDVI	0.49 ***	NGI	−0.57 ***
OSAVI	0.55 ***	MCCCI	0.64 ***
MNDI	0.64 ***	Mean	0.05
Entropy	0.50 ***	Variance	−0.01
Angular	−0.54 ***	Homogeneity	−0.40 ***
Dissimilarity	0.04	Contrast	−0.03
Correlation	−0.03		

Note: $p \leq 0.001$ (***).

The results of the correlation analysis between canopy SPAD values and texture features at the three key growth stages showed that at the jointing stage, significant redundancy existed among these features, with a correlation coefficient of −0.87 between entropy and angular second moment; entropy achieved the optimal correlation with SPAD ($r = 0.5$) in this period. The overall correlation between texture features weakened at the silking stage, while angular second moment and entropy showed the strongest correlation with SPAD ($r = -0.54$ and $r = 0.53$, respectively). The correlation between texture features and SPAD decreased overall at the grain-filling stage, with a maximum coefficient of only 0.38. Based on redundancy analysis, contrast and entropy were finally selected as the core texture indicators. Comparative verification showed that both texture features and VIs were significantly correlated with SPAD values.

3.3. SPAD Estimation Model Integrating VIs and Texture Features

Based on correlation analysis, we selected VIs (e.g., MCCCI) and texture features (Contrast, Entropy) strongly correlated with summer maize SPAD values and constructed canopy SPAD estimation models for the jointing, silking and grain-filling stages using multiple machine learning algorithms. The SVR model showed the best overall performance, and the integrated VIs and texture features significantly improved the SPAD prediction accuracy of all stages. At the jointing stage, single vegetation features outperformed texture features, and the integrated model further enhanced field stability. The integrated model reached a validation R^2 of 0.77 at the silking stage and maintained stable performance ($R^2 = 0.70$, $RMSE = 3.83$) at the grain-filling stage despite reduced single-feature accuracy caused by leaf senescence. This integrated strategy effectively compensates for single-feature limitations and enhances model generalization (Figure 5 and Table 5).

https://doi.org/10.3390/agriculture16131442

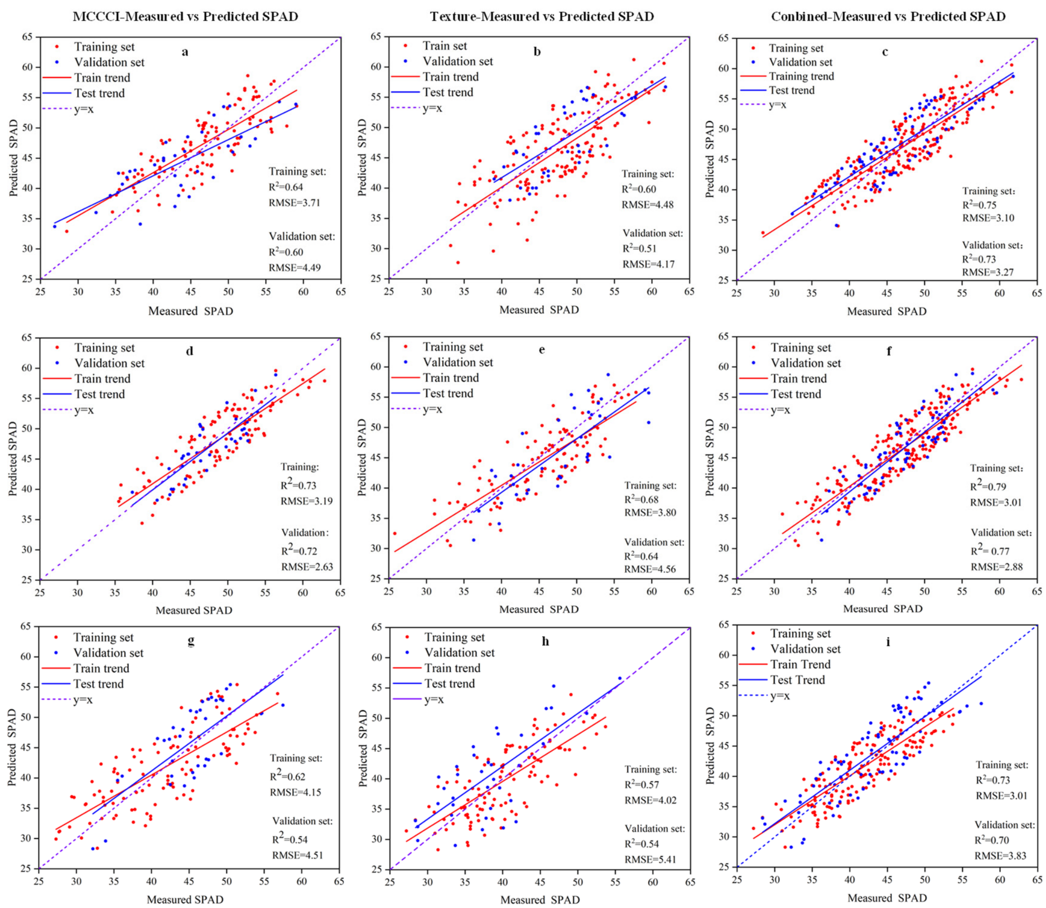

Figure 5. Comparison between simulated and measured SPAD results using image texture, vegetation indices, and their integration across different periods (blue represents the training set, and red represents the test set).(**a**) SPAD prediction using single vegetation index at the jointing stage; (**b**) SPAD prediction using single texture feature at the jointing stage; (**c**) SPAD prediction using combined features at the jointing stage; (**d**) SPAD prediction using single vegetation index at the silking stage; (**e**) SPAD prediction using single texture feature at the silking stage; (**f**) SPAD prediction using combined features at the silking stage; (**g**) SPAD prediction using single vegetation index at the grain-filling stages; (**h**) SPAD prediction using single texture feature at the grain-filling stages; (**j**) SPAD prediction using combined features at the grain-filling stages.

Table 5. Comparison of SPAD estimation models using vegetation indices and texture features.

Stage	Feature	Machine Learning Model	*RMSE*	*R²*
Jointing	Single vegetation feature	PLSR	4.30	0.45
		RF	5.49	0.11
		Linear Regression	4.30	0.45
		SVR	4.49	0.60
	Single texture feature	PLSR	4.88	0.42
		RF	5.15	0.41
		Linear Regression	5.04	0.42
		SVR	4.17	0.51
	Indictor System	PLSR	4.25	0.45
		RF	4.16	0.42
		Linear Regression	3.88	0.45
		SVR	3.27	0.73

https://doi.org/10.3390/agriculture16131442

To verify the superiority of the SPAD inversion model constructed in this study, comparative simulation analysis was conducted using jointing-stage data under different planting densities within the test set (Figure 6). All models performed stably under low density (PD6), with single VIs slightly outperforming single texture features. As density increased to PD9 and ultra-high-density PD12, the accuracy of single-feature models decreased significantly, especially the single texture feature model, whose inversion ability nearly failed under PD12, as canopy overlap and light heterogeneity from dense planting weakened texture feature sensitivity. In contrast, the integrated-feature model showed significant advantages in resisting density stress, with a significantly higher R^2 than single-feature models across all densities. It maintained a stable R^2 of 0.60–0.70 from PD3 to PD9 and retained an R^2 of 0.34 even under PD12. This study confirms that planting density is a key factor regulating the applicability of SPAD inversion models. The feature integration strategy offsets canopy structure interference via information complementarity between VIs and texture features, improving model generalization and the anti-interference ability for precise nutrition monitoring of densely planted maize.

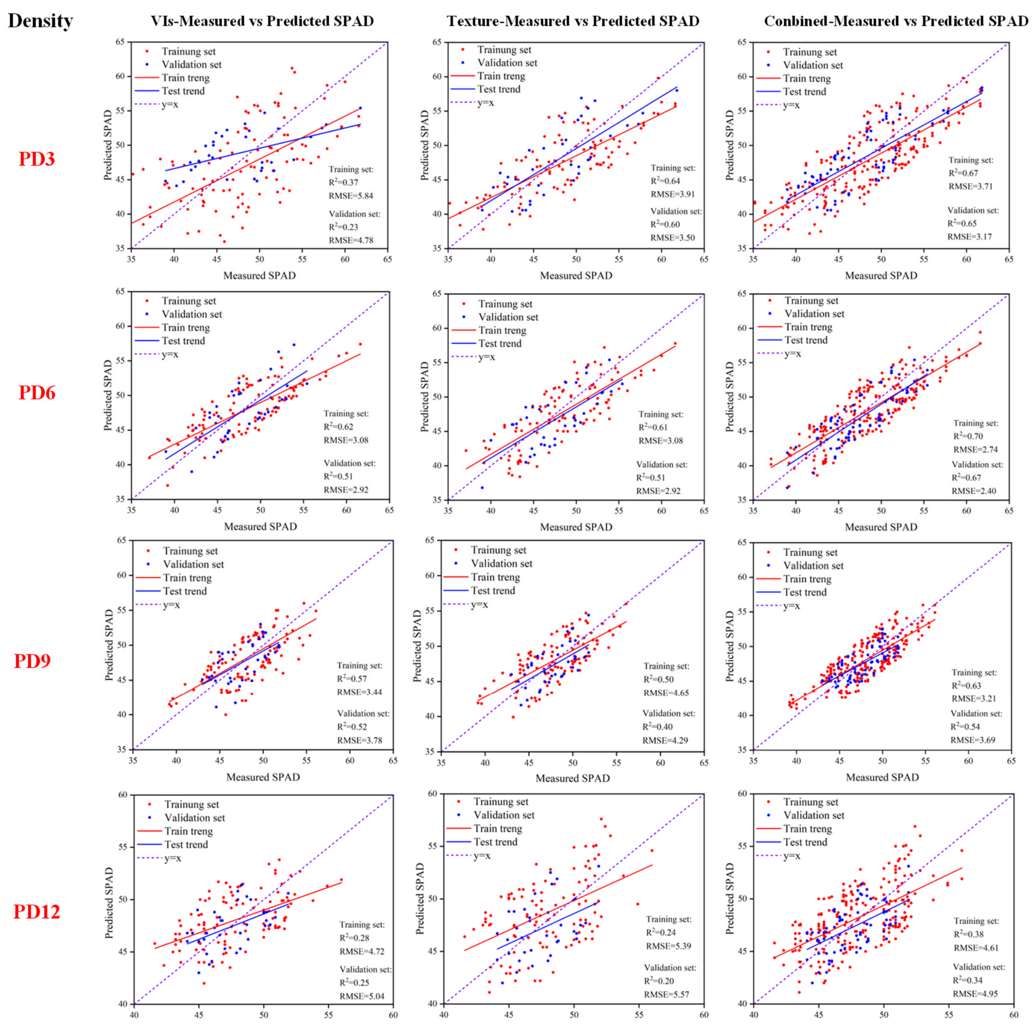

Figure 6. Comparison of feature types for SPAD inversion models at the jointing stage of maize under different planting densities. Note: PD3 (30,000 plants ha^{-1}), PD6 (60,000 plants ha^{-1}), PD9 (90,000 plants ha^{-1}), PD12 (120,000 plants ha^{-1}).

4. Discussion

4.1. Modeling the Differences Between VIs and Texture Features

In this study, compared with single-indicator methods, the integration of spectral and textural features consistently improves model accuracy across various algorithmic frameworks. A ternary integrated framework of "phenotypic feedback + management + environment" for maize above-ground biomass estimation was constructed by fusing multispectral, digital image and LiDAR data. The results revealed that the R^2 of the random forest model reached 0.92–0.93 under multimodal data fusion, representing a 15.8% improvement compared with the single vegetation index model [33]. To objectively evaluate the predictive performance of the proposed model and its research positioning in this field, we quantitatively compared our results with recent representative studies focusing on maize SPAD inversion using UAV multispectral remote sensing. Ma et al. (2024) estimated maize SPAD values under different irrigation regimes via PLSR, RF and SVR, achieving an optimal R^2 of 0.79 and an RMSE of 2.25 during the reproductive growth stage [4]. Parida et al. (2024) predicted maize SPAD using UAV-derived multispectral vegetation indices, with R^2 values of 0.83 for NDRE and 0.82 for MCARI [9]. In our study, the SVR model yielded an R^2 of 0.77 and an RMSE of 2.88 on the test set at the tasseling stage. When texture features were used for model construction, their prediction accuracy was slightly higher than that of spectral features during the early growth stage and after maize maturity. This improvement can be attributed to the inherent capabilities of texture features, which can amplify subtle spectral differences among ground objects; mitigate interference from background signals, the solar angle, and the sensor viewing angle; as well as suppress spectral variability. These features can further alleviate the impact of high crop coverage on spectral saturation during the inversion of growth indicators of multiple developmental stages. However, in the correlation analysis, spectral features consistently showed stronger associations with chlorophyll content compared to texture-based metrics. This phenomenon is attributed to the fact that the selected VIs relieves specific spectral bands, particularly the red-edge and near-infrared regions, which have a close correlation with chlorophyll content but also exhibit significant collinearity. Therefore, simply selecting highly correlated features as inputs may not improve modeling accuracy. The integration of spectral and textural features effectively alleviates the constraint of multicollinearity and compensates for the weak direct correlation between textural features and leaf chlorophyll content. This multi-feature fusion framework can stably enhance the prediction accuracy and generalization robustness of the SPAD inversion model, both throughout the full maize growth stage and under different planting density conditions.

4.2. UAV-Based Maize SPAD Estimation with SVR and Feature Screening

In our experiment, SPAD values estimated from UAV multispectral imagery showed strong agreement with ground measurements, with correlation coefficients exceeding 0.75, indicating good predictive performance. The small deviation between estimated and measured SPAD values may be partly attributable to the reduced influence of outliers when using canopy-level image statistics. For crop parameter inversion, both variable selection and the choice of machine learning algorithms are key determinants of model accuracy and stability. Selection strategies and algorithms differ in data processing, feature extraction, and training procedures, which directly affect inversion outcomes. Given the large number of image-derived features and potential multicollinearity, the relationships between spectral and texture features and chlorophyll content may shift after background removal. In this study, correlation analysis was used as an initial screening step to retain features closely related to SPAD values, which helped reduce dimensionality and mitigate multicollinearity. Based on the established indicator system, the SVR algorithm adopted in this study achieved a simulation accuracy of SPAD above 0.7 across different growth stages, which was significantly higher than that of single VIs and single texture features. Its estimation performance was also superior to other algorithms, enabling the extended estimation of maize SPAD under various planting densities. The VI-texture feature fusion framework constructed in this study shares a similar core concept with the multi-scale feature fusion design adopted in UAV-YOLO [34], namely, improving target representation capability through the complementarity of multi-source information. The SPPL module embedded in UAV-YOLO significantly strengthens the model's detection robustness against multi-scale objects by combining multi-scale pooling of SPPF with long-range dependency modeling via LSKA, achieving a 1.8% improvement in mAP@0.5. Similarly, the fusion of vegetation indices and texture features in our research effectively alleviates the spectral saturation limitation of single features during the canopy closure stage. Both approaches embody the modeling philosophy of synergistic integration of multi-scale and multi-source information.

4.3. Generalization of SPAD Inversion Model

In this work, we integrated machine learning approaches with multispectral data analysis to explore the generalization capabilities of the SPAD inversion model. SVR was employed to estimate SPAD values from a set of VIs. Experimental results demonstrated that the SVR model exhibits high reliability in key maize growth stages. While individual VIs offers valuable insights, their utility in SPAD inversion is constrained by limited predictive performance, making over-reliance on any single index a central challenge. Model complexity intensifies with a proliferation of VIs, raising computational expenses while heightening susceptibility to overfitting. To address these issues, we systematically analyzed the relationship between spectral indices and textural features with SPAD values, selecting the most relevant predictors for model construction according to the maize growth stage. There exists a significant linear relationship between SPAD values and the total nitrogen content of maize leaves. The field-scale spatial distribution map of SPAD values acquired by UAV can rapidly identify the spatial variability of nitrogen nutrition within fields. In practical field operations, the predicted SPAD values can be compared with pre-established nitrogen nutrition diagnostic criteria to evaluate the nitrogen surplus or deficiency status of maize plants. Planting density serves as the core regulating factor in this study, as canopy structure and nitrogen demand differ significantly across various density treatments; accordingly, predicted SPAD values can be directly adopted to formulate density-specific fertilization strategies. As a critical indicator of chlorophyll content, SPAD values directly reflect the photosynthetic capacity and nitrogen nutritional status of crops. The SPAD inversion model constructed from UAV multispectral remote sensing data enables rapid acquisition of canopy SPAD values at key maize growth stages, including the jointing, tasseling, and grain-filling stages. Using the SVR inversion model developed in this study and UAV multispectral imagery, we generated field-scale spatial distribution maps of canopy SPAD to reveal the spatial variability of nitrogen nutrition within individual fields. Remote sensing indicators and crop growth estimation provide spatially explicit crop status information for intelligent agricultural control systems, enabling the systems to generate differentiated management prescriptions accordingly, so as to achieve the organic integration of precise input and intelligent decision-making at the field scale [35]. The resulting SPAD inversion model exhibited strong generalization across different growth stages. Under the PD12 treatment, the canopy structure becomes extremely dense, leading to severe saturation of multispectral signals. The information captured by multispectral data is physically confined to the uppermost three to four leaf layers of the canopy. Variations in chlorophyll content within middle and lower leaves are masked by layered scattering during signal transmission, which alters the mapping relationship between model input features and the target variable. Shade-avoidance responses triggered by high planting density advance the peak value of the leaf area index and accelerate senescence of lower canopy leaves. The temporal decoupling between SPAD and LAI further degrades the model's predictive performance during the grain-filling stage. To improve model estimation accuracy under high planting density, a hierarchical modeling strategy can be adopted in future research, where a dynamic senescence function is incorporated alongside a density-aware module. By using planting density as an explicit input feature, the model can adaptively adjust feature weights according to different density levels. Furthermore, functional–structural plant models (FSPMs) can be employed to generate synthetic training datasets under various density regimes. Combined with transfer learning for model pre-training, prior physical knowledge derived from mechanistic models can be embedded into data-driven algorithms to strengthen the extrapolation capacity of the model under extremely dense planting conditions.

To address the inherent drawbacks of data-driven models, Physics-Informed Neural Networks (PINNs) can be introduced, whereby physiological laws such as carbon assimilation equations are embedded into the loss function as physical constraints to guarantee the biological rationality of predictions under extreme conditions. FSPMs can be utilized to generate virtual training datasets covering extreme planting density gradients. The transfer learning paradigm of "mechanism-based pre-training plus data fine-tuning" is adopted to compensate for the scarcity of field-measured samples under extreme conditions. Meanwhile, an active learning strategy is applied to identify extrapolation boundaries via predictive uncertainty, iteratively expand the training dataset with minimal sampling costs, and gradually broaden the effective extrapolation range of the model. For uncertainty quantification analysis, Monte Carlo Dropout is adopted to calculate the confidence interval of each predicted value and assign reliability labels to prediction outputs. Deep ensemble learning is employed to quantify the dispersion across different models, and spatial distribution maps of predictive uncertainty are plotted simultaneously. On this basis, a closed-loop framework of "prediction—validation—updating" is established. The quantified uncertainty results are directly used to optimize the layout of field validation sampling points, maximizing monitoring accuracy at the lowest sampling cost. This approach provides quantifiable reliability evaluation tools and operable iterative optimization pathways for the practical deployment of data-driven crop monitoring models.

4.4. Mechanistic Interpretation of Dynamic Correlations Between Spectral and Texture Features

As the maize growing season progresses, dynamic canopy structural evolution and physiological leaf senescence co-drive the temporal variations in the correlations between spectral–texture features and SPAD values, fundamentally determining model estimation performance across growth stages. At the jointing stage, sparse foliage induces prominent soil background interference. Benefiting from inherent sensitivity to pigment variation, red-edge indices (NDRE, MTCI) achieve high correlations (0.62–0.67) with leaf chlorophyll content and effectively characterize early SPAD dynamics. During tasseling and silking stages, rapid leaf expansion promotes canopy closure and severe leaf overlapping, triggering typical spectral saturation. When canopy visible-light absorption by chlorophyll reaches its physical limit, further pigment accumulation no longer produces distinct spectral responses. Although red-edge indices possess superior anti-saturation capability, persistent canopy occlusion weakens their pigment sensitivity, decreasing their correlation coefficients to 0.55. At the grain-filling stage, complete canopy closure causes severe saturation of conventional indices such as NDVI. In contrast, ratio-based indices (RVI, VIopt, OSAVI) mitigate structural interference via optimized band combinations and soil adjustment, maintaining stable correlations above 0.75 with SPAD. Synchronously, texture features exert unique complementary advantages. When spectral signals lose discriminative capacity under saturation, entropy and contrast quantify canopy spatial heterogeneity, including leaf arrangement, overlap degree and shadow distribution. Providing orthogonal structural information independent of spectral pigment characteristics, texture features compensate for spectral information loss and enrich multi-dimensional SPAD inversion inputs. Late-stage leaf senescence further reshapes feature correlations. Early chlorophyll degradation induces a red-edge blue shift, markedly reducing the reliability of red-edge indices. In middle and late senescence, destroyed leaf cellular structures homogenize canopy texture and weaken near-infrared differentiation, thereby degrading texture feature performance. Genotypic stay-green traits and nitrogen management regulate senescence rates and further stabilize stage-dependent feature correlations. High planting density accelerates canopy closure and advances spectral saturation. Severe canopy homogenization renders single texture-based models ineffective, while the fusion model retains a satisfactory R^2 of 0.34. This demonstrates that spectral texture fusion effectively alleviates saturation and occlusion interference. Overall, spectral features reflect physiological pigment variations, while texture features compensate for structural defects of saturated spectra, verifying the mechanistic rationality and boundary adaptability of multi-feature collaborative modeling for maize SPAD dynamic monitoring.

5. Conclusions

This study utilized UAV multispectral imagery to establish a non-destructive estimation of canopy SPAD values during maize growth under various planting densities. This study collected 12,240 multispectral images for establishing datasets during the growth period under different planting densities in the two-year experiment. The indicator system was constructed using 18 VIs and eight texture features to analyze the correlations with SPAD values. The detection accuracy of three algorithms (SVR, RF, PLSR) was compared under single features and feature integration. The results show that the red-edge and near-infrared bands are most sensitive to changes in SPAD values estimation. Canopy spectral characteristics vary significantly with the growth stage, and no single feature can provide reliable estimation during the growth period. Based on the SVR algorithm and the constructed indicator system, the proposed model achieves high estimation accuracy and strong generalization capability throughout the maize entire growth period. This model effectively improves the inversion accuracy of canopy SPAD values, laying a solid technical foundation for precise nitrogen nutrient management in summer maize cultivation. Furthermore, the feasibility of using the SVR algorithm combined with this indicator system to simulate maize SPAD under different planting densities was also validated.

Supplementary Materials: The following supporting information can be downloaded at: https://www.mdpi.com/article/10.3390/agriculture16131442/s1, Figure S1: XGBoost-based direct yield prediction model using vegetation indices from the jointing stage; Figure S2: XGBoost-based direct yield prediction model using vegetation indices from the silking stage; Figure S3: XGBoost-based direct yield prediction model using vegetation indices from the grain-filling stage.

Author Contributions: Writing—review and editing, Formal analysis, C.L.; Data curation, L.D.; Data curation, Z.Z.; Data curation, J.H.; Investigation, Data curation, H.L.; Writing—review and editing, Supervision, S.J.; Writing—review and editing, Supervision, Y.S.; Writing—review and editing, Supervision, J.L.; Funding acquisition, Y.S. and J.L. All authors have read and agreed to the published version of the manuscript.

Funding: The authors gratefully acknowledge the financial support provided by the National Key R&D Program of China: Integrated Technical Model and Application for Productivity Improvement of Lime Concretion Black Soil in the Huaihe River Basin (2023YFD1901000).

Institutional Review Board Statement: Not applicable.

Informed Consent Statement: Not applicable.

Data Availability Statement: The raw data supporting the conclusions of this article will be made available by the authors on reasonable request.

Conflicts of Interest: The authors declare no conflicts of interest.

References

1. Erenstein, O.; Jaleta, M.; Sonder, K.; Mottaleb, K.; Prasanna, B.M. Global maize production, consumption and trade: Trends and R&D implications. *Food Secur.* **2022**, *14*, 1295–1319. https://doi.org/10.1007/s12571-022-01288-7.
2. Silva, L.; Conceição, L.A.; Lidon, F.C.; Maçãs, B. Remote monitoring of crop nitrogen nutrition to adjust crop models: A aeview. *Agriculture* **2023**, *13*, 835. https://doi.org/10.3390/agriculture13040835.
3. Szulc, P.; Bocianowski, J.; Nowosad, K.; Zielewicz, W.; Kobus-Cisowska, J. SPAD Leaf greenness index: Green mass yield indicator of maize (*Zea mays* L.), genetic and agriculture practice relationship. *Plants* **2021**, *10*, 830. https://doi.org/10.3390/plants10050830.
4. Ma, W.; Han, W.; Zhang, H.; Cui, X.; Zhai, X.; Zhang, L.; Shao, G.; Niu, Y.; Huang, S. UAV multispectral remote sensing for the estimation of SPAD values at various growth stages of maize under different irrigation levels. *Comput. Electron. Agric.* **2024**, *227*, 109566. https://doi.org/10.1016/j.compag.2024.109566.
5. Ludwig, A.D.; Doktor, D.; Goss, R.; Sasso, S.; Feilhauer, H. The leaf is always greener on the other side of the lab: Optical in-situ indicators for leaf chlorophyll content need improvement for semi-natural grassland areas. *Ecol. Indic.* **2022**, *143*, 109424. https://doi.org/10.1016/j.ecolind.2022.109424.
6. Zhang, Z.; Zhu, L. A Review on Unmanned Aerial Vehicle remote sensing: Platforms, sensors, data processing methods, and applications. *Drones* **2023**, *7*, 398. https://doi.org/10.3390/drones7060398.
7. Feng, L.; Chen, S.; Zhang, C.; Zhang, Y.; He, Y. A comprehensive review on recent applications of unmanned aerial vehicle remote sensing with various sensors for high-throughput plant phenotyping. *Comput. Electron. Agric.* **2021**, *182*, 106033. https://doi.org/10.1016/j.compag.2021.106033.
8. Wu, Q.; Zhang, Y.; Zhao, Z.; Xie, M.; Hou, D. Estimation of relative chlorophyll content in spring wheat based on multi-temporal UAV remote Sensing. *Agronomy* **2023**, *13*, 211. https://doi.org/10.3390/agronomy13010211.
9. Parida, P.K.; Somasundaram, E.; Krishnan, R.; Radhamani, S.; Sivakumar, U.; Parameswari, E.; Raja, R.; Shri Rangasami, S.R.; Sangeetha, S.P.; Gangai Selvi, R. Unmanned Aerial Vehicle-Measured Multispectral Vegetation Indices for Predicting LAI, SPAD Chlorophyll, and Yield of Maize. *Agriculture* **2024**, *14*, 1110. https://doi.org/10.3390/agriculture14071110.
10. Kyratzis, A.C.; Skarlatos, D.P.; Menexes, G.C.; Vamvakousis, V.F.; Katsiotis, A. Assessment of vegetation indices derived by UAV imagery for durum wheat phenotyping under a water limited and heat stressed mediterranean environment. *Front. Plant Sci.* **2017**, *8*, 1114. https://doi.org/10.3389/fpls.2017.01114.
11. Liu, Y.; Feng, H.; Yue, J.; Fan, Y.; Bian, M.; Ma, Y.; Jin, X.; Song, X.; Yang, G. Estimating potato above-ground biomass by using integrated unmanned aerial system-based optical, structural, and textural canopy measurements. *Comput. Electron. Agric.* **2023**, *213*, 108229. https://doi.org/10.1016/j.compag.2023.108229.
12. Jamil, M.D.; Abbas, M.Z.; Saeed, M.F.; Jamal, A.; Mubeen, M.; Zakir, A.; Ahmad, I.; Jameel, R.; Pentoś, K.; Dewir, Y.H.; et al. Improved early-stage crop classification using a novel fusion-based machine learning approach with Sentinel-2A and Landsat 8–9 data. *Environ. Monit. Assess.* **2025**, *197*, 982. https://doi.org/10.1007/s10661-025-14420-9.
13. Wang, S.; Wang, B.; Zheng, J.; Tuerxun, N.; Wang, R.; Zhang, K.; Xu, Y.; Yang, Y. Contributions of multiple UAV features to cotton SPAD estimation from the perspective of explainable machine learning. *Agriculture* **2026**, *16*, 325. https://doi.org/10.3390/agriculture16030325.
14. Nguyen, C.; Sagan, V.; Skobalski, J.; Severo, J.I. Early detection of wheat yellow rust disease and its impact on terminal yield with multi-spectral UAV-imagery. *Remote Sens.* **2023**, *15*, 3301. https://doi.org/10.3390/rs15133301.
15. Huete, A.; Didan, K.; Miura, T.; Rodriguez, E.P.; Gao, X.; Ferreira, L.G. Overview of the radiometric and biophysical performance of the MODIS vegetation indices. *Remote Sens. Environ.* **2002**, *83*, 195–213. https://doi.org/10.1016/S0034-4257(02)00096-2.
16. Tian, Y.C.; Yao, X.; Yang, J.; Cao, W.X.; Hannaway, D.B.; Zhu, Y. Assessing newly developed and published vegetation indices for estimating rice leaf nitrogen concentration with ground- and space-based hyperspectral reflectance. *Field Crops Res.* **2011**, *120*, 299–310. https://doi.org/10.1016/j.fcr.2010.11.002.

17. Haboudane, D.; Miller, J.R.; Pattey, E.; Zarco-Tejada, P.J.; Strachan, I.B. Hyperspectral vegetation indices and novel algorithms for predicting green LAI of crop canopies: Modeling and validation in the context of precision agriculture. *Remote Sens. Environ.* **2004**, *90*, 337–352. https://doi.org/10.1016/j.rse.2003.12.013.
18. Candiago, S.; Remondino, F.; De Giglio, M.; Dubbini, M.; Gattelli, M. Evaluating multispectral images and vegetation indices for precision farming applications from UAV images. *Remote Sens.* **2015**, *7*, 4026–4047. https://doi.org/10.3390/rs70404026.
19. Daughtry, C.S.T.; Walthall, C.L.; Kim, M.S.; de Colstoun, E.B.; McMurtrey, J.E. Estimating corn leaf chlorophyll concentration from leaf and canopy reflectance. *Remote Sens. Environ.* **2000**, *74*, 229–239. https://doi.org/10.1016/S0034-4257(00)00113-9.
20. Liu, J.; Pattey, E.; Jégo, G. Assessment of vegetation indices for regional crop green LAI estimation from Landsat images over multiple growing seasons. *Remote Sens. Environ.* **2012**, *123*, 347–358. https://doi.org/10.1016/j.rse.2012.04.002.
21. Laosuwan, T.; Uttaruk, Y. Carbon sequestration assessment of the orchards using satellite data. *J. Ecol. Eng.* **2017**, *18*, 11–17. https://doi.org/10.12911/22998993/66257.
22. Sripada, R.P.; Heiniger, R.W.; White, J.G.; Weisz, R. Aerial color infrared photography for determining late-season nitrogen requirements in Corn. *Agron. J.* **2005**, *97*, 1443–1451. https://doi.org/10.2134/agronj2004.0314.
23. Wu, W. The Generalized Difference Vegetation Index (GDVI) for dryland characterization. *Remote Sens.* **2014**, *6*, 1211–1233. https://doi.org/10.3390/rs6021211.
24. Schuerger, A.C.; Capelle, G.A.; Di Benedetto, J.A.; Mao, C.; Thai, C.N.; Evans, M.D.; Richards, J.T.; Blank, T.A.; Stryjewski, E.C. Comparison of two hyperspectral imaging and two laser-induced fluorescence instruments for the detection of zinc stress and chlorophyll concentration in bahia grass (*Paspalum notatum* Flugge.). *Remote Sens. Environ.* **2003**, *84*, 572–588. https://doi.org/10.1016/S0034-4257(02)00181-5.
25. Richardsons, A.J.; Wiegand, A.J.P.E.; Sensing, R. Distinguishing vegetation from soil background information. *Photogramm. Eng. Remote Sens.* **1977**, *43*, 1541–1552.
26. Chen, J.M. Evaluation of vegetation indices and a modified simple ratio for boreal applications. *Can. J. Remote Sens.* **1996**, *22*, 229–242. https://doi.org/10.1080/07038992.1996.10855178.
27. Graeff, S.; Claupein, W. Quantifying nitrogen status of corn (*Zea mays* L.) in the field by reflectance measurements. *Eur. J. Agron.* **2003**, *19*, 611–618. https://doi.org/10.1016/S1161-0301(03)00007-8.
28. Fitzgerald, G.J. Characterizing vegetation indices derived from active and passive sensors. *Int. J. Remote Sens.* **2010**, *31*, 4335–4348. https://doi.org/10.1080/01431160903258217.
29. Dash, J.; Curran, P.J. The MERIS terrestrial chlorophyll index. *Int. J. Remote Sens.* **2004**, *25*, 5403–5413.
30. Gitelson, A.A.; Viña, A.; Verma, S.B.; Rundquist, D.; Arkebauer, T.J.; Keydan, G.P.; Leavitt, B.; Ciganda, V.S.; Burba, G.; Suyker, A.E. Relationship between gross primary production and chlorophyll content in crops: Implications for the synoptic monitoring of vegetation productivity. *J. Geophys. Res. Atmos.* **2006**, *111*, D08S11.
31. Reyniers, M.; Walvoort, D.J.J.; De Baardemaaker, J. A linear model to predict with a multi-spectral radiometer the amount of nitrogen in winter wheat. *Int. J. Remote Sens.* **2006**, *27*, 4159–4179. https://doi.org/10.1080/01431160600791650.
32. Datt, B. Visible/near infrared reflectance and chlorophyll content in Eucalyptus leaves. *Int. J. Remote Sens.* **1999**, *20*, 2741–2759. https://doi.org/10.1080/014311699211778.
33. Feng, Z.; Yang, Z.; Suo, L.; Wu, K.; Ma, Z.; Zhang, H.; Duan, J.; Feng, W. Enhancing maize above-ground biomass estimation through multispectral, digital and LiDAR fusion on UAV platforms. *Agric. Water Manag.* **2025**, *315*, 109551. https://doi.org/10.1016/j.agwat.2025.109551.
34. Di, X.; Cui, K.; Wang, R.-F. Toward efficient UAV-based small object detection: A lightweight network with enhanced feature fusion. *Remote Sens.* **2025**, *17*, 2235. https://doi.org/10.3390/rs17132235.
35. Tu, Y.-H.; Wang, R.-F.; Su, W.-H. Active disturbance rejection control—new trends in agricultural cybernetics in the future: A comprehensive review. *Machines* **2025**, *13*, 111. https://doi.org/10.3390/machines13020111.